Predicted electronic markers for polytypes of LaOBiS_{2} examined via angle-resolved photoemission spectroscopy

Xiaoqing Zhou, Qihang Liu, J. A. Waugh, Haoxiang Li, T. Nummy, Xiuwen Zhang, Xiangde Zhu, Gang Cao, Alex Zunger, and D. S. Dessau

Phys. Rev. B **95**, 075118 — Published 9 February 2017

DOI: 10.1103/PhysRevB.95.075118

Predicted electronic markers for polytypes of $LaOBiS_2$ examined via angular resolved photoemission spectroscopy

Xiaoqing Zhou,[1] Qihang Liu,[2*] J. A. Waugh,[1] Haoxiang Li,[1] T. Nummy,[1] Xiuwen Zhang,[2] Xiangde Zhu,[3] Gang Cao[4], Alex Zunger[2*] and D. S. Dessau[1,2*]

[1]Department of Physics, University of Colorado at Boulder, CO 80309, USA

[2]Renewable and Sustainable Energy Institute, University of Colorado at Boulder, CO 80309, USA

[3]High Magnetic Field Laboratory of the Chinese Academy of Sciences, Hefei, China

[4]University of Kentucky, Lexington, KY 40506, USA

[*]E-mail: qihang.liu85@gmail.com; daniel.dessau@colorado.edu; alex.zunger@colorado.edu.

Abstract

The natural periodic stacking of symmetry-inequivalent planes in layered compounds can lead to the formation of natural superlattices; albeit close in *total* energy, (thus in their thermodynamic stability), such polytype superlattices can exhibit different structural symmetries, thus have markedly different electronic properties which can in turn be used as "structural markers". We illustrate this general principle on the layered $LaOBiS_2$ compound where density-functional theory (DFT) calculations on the $(BiS_2)/(LaO)/(BiS_2)$ polytype superlattices reveal both qualitatively and quantitatively distinct electronic structure markers associated with the Rashba physics, yet the *total* energies are only ~ 0.1 meV apart. This opens the exciting possibility of identifying subtle structural features via electronic markers. We show that the pattern of removal of band degeneracies in different polytypes by the different forms of symmetry breaking leads to new Rashba "mini gaps" with characteristic Rashba parameters that can be determined from spectroscopy, thereby narrowing down the physically possible polytypes. By identifying these distinct DFT-predicted fingerprints via ARPES measurements on $LaBiOS_2$ we found the dominant polytype with small amounts of mixtures of other polytypes. This conclusion, consistent with neutron scattering results, establishes ARPES detection of theoretically established electronic markers as a powerful tool to delineate energetically quasidegenerate polytypes.

I. Introduction

Ordered crystalline compounds of fixed composition are generally assumed to have a unique and specific crystallographic structure being distinctly separate from other phases in the low-temperature phase diagram. An exception is *polytypes* that represent an energetically closely spaced set of ordered compounds with the same composition often differing by orientations of certain sub-units. The best know example is zinc-blend and wurtzite polytypes of binary semiconductors[1] best exemplified by SiC that show ~100 polytypes[2], or ZnO, ZnS appearing each as either zinc-blend or wurtzite. What makes such polytypes electronically interesting is that despite a tiny difference in their thermodynamic stability (usually, the total energy difference is only in the order of less than 10 meV/atom[3]) their electronic properties can differ significantly. For example, the difference on band gap of SiC 4H and 3C polytypes is almost 1 eV[4] and the wurtzite form of III-V nitrides is polar whereas 3C is nonpolar, a distinction that alters profoundly the electric field profile in nitride lasers and light emitting diodes[5].

With the recent interest in the condensed matter physics community of layered two-dimensional (2D) compounds such as graphene[6], the transition metal dichalcogenides[7], and topological insulators[8], the stacking sequences of these layers is expected to take on a new importance. This is especially important in cases where the individual 2D layers exhibit structural distortions (such as inequivalent in-plane bonds), the stacking of which along the perpendicular direction creates "*natural superlattices*". Because of the great similarity in their *thermodynamic energies*, polytype physics is rather difficult to explore by conventional structural probes. Yet, various stacking sequences may maintain or break inversion symmetry that can then play an important role in keeping or lifting certain degeneracies, with implications for their electronic structure, spin polarization physics and Rashba physics. How to characterize and understand these 'electronic markers' has only been minimally addressed, either theoretically or experimentally.

As an important prototype system we focus on the layered oxides of the type $(BiS_2)/(LaO)/(BiS_2)$ where the 2D planes of BiS_2 are separated from each other by the LaO barrier (Fig. 1a). This material has recently received a good deal of interest because of its potential to host unconventional superconductivity up to 10.6 K[9], hidden spin polarizations[10, 11], spin field effect transistors[12] and electrically tunable Dirac cones[13], etc. In the previous studies, the compound was often assumed to have a centrosymmetric space group of P4/nmm, and to have a single specific crystallographic structure (called T_0 here)[14-16]. However, such high-symmetry structure having two equal in plane Bi-S bonds reported in the Inorganic Crystal Structure Database (ICSD) database has been predicted by Yildirim to

be dynamically unstable[17], and further neutron diffraction experiment[18] confirmed that the two Bi-S bonds have different lengths. Some of the present authors[19] examined via density functional theory (DFT) various polytype arrangements of the individual 2D planes having unequal Bi-S bonds and predicted three stable classes of polytypes (noted as T_1-T_3), some being centrosymmetric and some breaking inversion symmetry (Fig. 1b). Although superconductivity (but not polytypes) of n-type doped $LaBiO_2$ attracts a lot of research interests[9], in this paper we focus on this newly discovered effect of polytypism in the un-doped material without the structural evolution[18] introduced by F-doping. We show that such polytypes give rise to distinctly different symmetry-related electronic properties, even though their total energies are quasidegenerate[6]. For example, whereas in the T_0 structure there is a crossing of two doubly degenerate bands (so the crossing point is 4-fold degenerate, see Fig. 2a) due to its relatively higher symmetry, in other polytypes we predict two characteristic types of (partial) degeneracy removal (Fig. 2a) at X and Y points of the rectangular-shaped Brillouin zone (BZ), leading to the formation of internal "mini-gaps" within the valence band or the conduction band. In addition, the Rashba bands manifest minima at different wavevectors for different polytypes. By considering the electronic structure of different polytypes we discover certain "electronic markers" that are predicted to be sensitive to polytype stacking and the ensuing symmetry. Thus, measurements of such markers can be used in conjunction with theory, to determine structure; thereby complementing information from conventional structural probes (diffraction). Here we present detailed angle-resolved photoemission spectroscopy (ARPES) results of this system, aiming for identifying the possible polytype physics in this system. Notably, ARPES provides us with the detailed band structure to be compared with DFT calculations based on different polytypes. Our work establishes spectroscopic detection of theoretically established electronic markers as a powerful tool to delineate energetically quasi-degenerate polytypes.

II. Methods

DFT calculations: The equilibrium crystal structure was obtained by DFT total energy minimization performed with an energy tolerance of 10^{-4} eV, and all atomic positions were relaxed with a force tolerance of 10^{-3} eV/Å. The electronic structures were calculated by using the projector-augmented wave (PAW) pseudopotential[20] and the exchange and correlation of Perdew, Burke, and Ernzerfhof (PBE)[21] as implemented in the Vienna *ab initio* package (VASP)[29]. The plane wave energy cutoff (reflecting basis set size) was set to 550 eV. Spin-orbit coupling was included as a perturbation to the

pseudopotential throughout the calculation. We note that he PBE functional didn't take the long-range van der Waals (VDW) interaction into account, and thus usually overestimate the interlayer space. However, the VDW correction underestimates the in-plane lattice constant and thus causes the T_0 structure to be the ground state, which contradicts the theoretical prediction and experiments. Since the accuracy of the in-plane lattice constant is more important to investigate the polytype physics, we used PBE functional for the base of calculation and analysis.

Sample Growth: High-quality single crystals of LaBiOS2 were grown using CsCl/KCL as flux. The charge was sealed in a quartz tube, fired at 850 ^{o}C and then slowly cooled down to room temperature. The technique is similar to that described in Ref.24. The size of the single crystals studied is of order 2.0 x 2.0 x 0.3 mm^3. The **chemical composition** of each single-crystal studied was determined using energy dispersive X-ray analysis (EDX) (Hitachi/Oxford 3000). Each sample studied is confirmed to be stoichiometrically consistent with $LaBiOS_2$. EDX and XRD results indicate that the quality of single crystals is uniform, and the crystal cleaves easily with very flat cleaved surface. Although in the present work we did not perform structure determination, the structural analysis of neutron diffraction data can be found elsewhere[22].

Photoemission: ARPES measurements have been carried out at Advanced Light Source (ALS) beam line 10.0.1 and 4.0.3, as well as Swiss Light Source beamline 9L with combinations of multiple beam energies (30 eV to 120 eV, every 10 eV), sample geometries (incoming light along high symmetry line Γ-X, Γ-Y and Γ-M), beam spot sizes (down to 30*100 μm^2 at ALS 4.0.3 and at SLS), and light polarizations (linear horizontal, linear vertical, circular right and circular left). All the data appear to be consistent with the polytype scenario with different matrix element effects.

III. Predicted electronic markers of different $LaOBiS_2$ polytypes

The basic layered crystal structure of $LaOBiS_2$ is shown in Fig. 1a, with a sandwiched structure containing two BiS_2 layers and an intermediate LaO layer. The structure (referred as "T_0") has high symmetry (space group #129, P4/nmm) with the x-y in-plane Bi and S atoms forming a perfect square (Fig. 1b). However, T_0 structure was predicted to have phonon instability via first-principle calculations[17]. Instead, an in-plane distortion causing alternation of the length of the Bi-S bonds could stabilize the structure. Considering the stacking of two BiS_2 layers along the z direction, one can get three polytypes by stacking layers whose Bi-S bonds are distorted along different direction (Fig. 1b) : (i) both layers distort along the x direction [(x, x), referred as polytype "T_1"]; (ii) one layer distorts along

the x direction while the other along –x direction [(x, -x), referred as polytype "T_2"], and (iii) one layer distorts along the x direction while the other along y direction [(x, y), referred as polytype "T_3"]. All the polytypes T_1-T_3 are almost equally likely to exist in a real sample as their energy differences are quite small (~ 0.1 meV per atom[19]). The stacking direction, space group and the presence of inversion symmetry for T_0-T_3 structure are listed in Table I. Neglecting the small energy difference between polytypes, the (x, y) orientation of T_3 has twice the occurrence probability of T_1 (x, x) or T_2 (x, -x) but the actual mixture in a real sample could be controlled by growth effects (e.g., the interfacial energies between polytypes and growth rates).

We use DFT in the electronic structure calculation with the projector-augmented wave (PAW) pseudopotential[20] and the exchange and correlation of Perdew, Burke, and Ernzerfhof (PBE)[21]. The equilibrium crystal structures are obtained by DFT total energy minimization (see Methods for more details). We note the following electronic markers of polytypism:

(i) Formation of polytype-dependent Rashba mini gap at the X or Y wavevectors in the BZ: Among the 4 polytypes considered here, T_0 has the highest symmetry with a non-symmorphic and centrosymmetric space group P4/nmm. Even though the combination of the two BiS_2 layers in a unit cell creates a centrosymmetric structure, the system produces a Rashba-like splitting due to the locally non-centrosymmetric nature of each BiS_2 sector, leading to two Rashba-like bands with opposite helical spin topology[11]. The two band crossing points at wavevectors X(Y) are superimposed by screw axis operation along the x(y) real space direction, leading to 4-fold degeneracy (including spin). The effective Hamiltonian around the wavevector X involves a 4x4 Dirac matrix, rendering a 3D Dirac cone (on a small energy scale near the degeneracy point) robust even with spin-orbit coupling (SOC)[23, 24]. On the other hand, the bands off the X(Y) wavevectors are all two-fold degenerate due to inversion symmetry and time reversal symmetry. The result is two horizontally shifted parabolas crossing at one point; we refer to this type of band structure feature as "band motif I", shown in Fig. 2a. Each polytype has two band motifs—one at X and one at Y. DFT calculation verifies that in T_0 polytype the BM of both X and Y valley are the same and belong to type I, as shown in Fig. 2b.

However, such Dirac points are not robust against symmetry-lowering perturbations. When the dynamically unstable T_0 evolves to its polytypes T_1-T_3, it looses non-symmorphic symmetries and thus removes the 4-fold degeneracy of Dirac points at certain valleys, forming internal "mini-gaps" within the valence and conduction bands. For T_1 (space group $Pmn2_1$) structure, the remaining symmetry

operation that can protect the Dirac point is the screw axis $\{C_{2x}|(1/2, 0, 0)\}$, so it ensures Dirac cones at X, while due to the loss of $\{C_{2y}|(1/2, 0, 0)\}$ symmetry at Y point the 4-fold degeneracy splits into two Kramers pairs with a mini-gap between the splitted bands (see Fig. 2c). Thus, the X point has BM–I whereas the Y point has BM-II. On the other hand, T_2 (space group $P2_1/m$) has $\{C_{2y}|(1/2, 0, 0)\}$ symmetry and thus hosts Dirac points at Y and gapped states at X (see Fig. 2d). The BM having such a mini-gap at X(Y) instead of a Dirac point is "type II BM" schematically shown in Fig. 2a. Type II BM could have 2-fold degenerate bands off X(Y) due to inversion symmetry (as in T_2), or singly-degenerate bands off X(Y) due to the absence of inversion symmetry (as in T_1). Finally, T_3 has the lowest symmetry C2 without inversion or non-symmorphic symmetry, rendering identical gapped states at both X and Y (see Fig. 2e).

Figure 2f summarizes the BM types of X and Y valley for T_0-T_3 polytypes, showing that according to the classification by the degree of degeneracy of the high-symmetry wavevectors, each of the 4 polytypes T_0-T_3 has a unique BM(X) and BM(Y). We further note that the polytype T_1 that has a real-space (y, y) stacking and T_2 with a real space (x, -x) stacking have each one BM-I and one BM-II, so they are indistinguishable if one considers only the band motifs at the individual X and Y wavevectors. But these polytypes would be distinct if we add the marker "mini-gap" Δ for different bands and valleys, illustrating distinct markers for different polytypes. For example, for T_1 the mini-gap of conduction band Δ_{CB} is larger than that of the valence band Δ_{VB}, while for T_2 the minigap Δ_{CB} is smaller than Δ_{VB}. For T_3 the X and Y valleys are symmetric (see Table I).

(ii) ***The minima of the Rashba bands occur in different wavevectors for different polytypes:*** The classical Rashba spin splitting manifests two parabolic band dispersions shifting towards each other in momentum space. The band edges located off the high-symmetry point are shown in Fig. 2a. In BM type I of centrosymmetric structures (T_0 and T_2), the band splitting along Γ-X (Γ-Y) high-symmetry line that locates inside the BZ is due to the combined contribution of the hybridization between two BiS_2 layers and SOC, indicating a larger momentum offset. In contrast, along X-M (Y-M) located at the surface of the BZ the band splitting is purely SOC-induced, while the layer hybridization is forbidden by the non-symmophic symmetry. This effect is stronger for conduction bands in which the momentum offset along Γ-X is 3-4 times larger than that along X-M direction, as shown in Fig. 2. On the other hand, for the non-centrosymmetric polytypes especially T_3, the anisotropy of momentum offset along different symmetry lines is strongly suppressed. The band edges of both conduction band and valence band of the polytypes are distinctly located at different wavevectors, as shown also in Table I. The dispersions of the

conduction bands and the valence bands, especially the band edges in momentum space could be a marker for identification by ARPES spectra.

IV. Band structure, dispersion and Fermi surface - electronic markers from ARPES

Figure 3a shows the ARPES measured Fermi map in the first Brillouin zone, with four small electron pockets found at the X/Y points, which generally agree with the theoretical predictions, as well as previous measurements[25, 26] on F-doped compounds. Fig. 3b shows an example of the zoomed-in spectra on one of the electron pockets, with decreasing intensity in the second Brillouin zone. The Fermi surface around the X, Y points form two contour loops with a nearly square shape, indicating the Rashba band splitting. The band dispersions for the conduction bands and valence bands along the high symmetry cut Γ-Y and X-M direction are shown in Fig. 3c.

From these we see that the band gap between the CB and VB is about 0.9 eV and that the sample is lightly doped n-type. This unintentional doping suggests the existence of donor defects, (such as anion vacancies or donor anti-site defects). Had they existed in high (e.g., percent) concentration, this might contriute to spectral broadening. This unintentional doping is manifested by a shift of the Fermi energy above that of the compensated material, and allows a clear view of both the conduction and valence bands with ARPES without the complication introduced by F-substituting.

We note that F substitution (indeed, alloying) is different because it occures on ~ 50% level which has been shown to lack a symmetry breaking distortion in the Bi-S plane[17, 18, 27] as well as to modify charge fluctuations and phonon modes. The photoemission observed band splitting along Γ-X is obvious whereas the splitting along X-M is negligible[16, 25]. According to the analysis of the present paper the 50 % alloyed compound of $LiOFBiS_2$ is most likely a new compound in its own righ, with another kind of in-plane distortion and thus different polytypes.

As shown in Fig. 3c, there are a clear distinction between X/Y pockets, which implies the existence of T1/T2 as such a distinction is a prediction of the polytype scenarip for the T_1/T_2 cases. Nevertheless, there could still be a concern that the X and Y points shown here were not taken under the identical geometrical conditions, i.e. with the same matrix elements. To verify that the anisotropy between X/Y pockets is not related to the matrix element effect at all, we have repeated the experimental study by only rotating the sample in azimuth angle by 90° and hence switching Γ-X to Γ-Y, as shown in Fig. 4 (note that this geometry is somewhat different from that used in Fig. 3). Under such conditions the matrix element effects must be the same between the two cuts in this figure, so the clear differences

between these cuts shows the distinction between the X and Y pockets, which has to arise from the polytypism.

Examples of the zoomed-in spectra of the conduction bands and valence bands along the high symmetry direction M-X-M and Y-Γ-Y are presented in Fig. 5, to be compared with DFT predictions of T_0, T_1, T_2 and T_3 respectively. A few observations are made in the following: (1) the typically assumed structure (single T_0 polytpe) is not able to explain the data; (2) the data supports a superposition of polytpes as no single polytpe can explain all the data; and (3) the dominant polytpe appears to be T_3 type as this captures the majority of the major features even though T_1/T_2 might also exist.

For the CB spectrum along M-X-M the experimental data (top left) shows a clear internal or central state that is absent in the calculated spectrum for T_0, as marked by the arrow in the 2nd panel down, left column. This is a clear marker that we need to go beyond the simplest structure (T_0 polytype). The other polytypes T_1, T_2, and T_3 as calculated for this cut all show the central state, though the differences between the calculated structures for this cut are similar enough that we should look to other cuts to distinguish between these possibilities.

On the other hand, the experimental conduction band minima shown in Figs. 4a and 4b are at very much the same energy, which is at odds with the theoretical prediction of a significant anisotropy of the CB minimum for both the T_1 and T_2 polytypes, as highlighted in columns a and b. We note that the energy difference of the CB minima for polytpes T_1 and T_2 is a few hundred meV different than for T0 and T3, even though the overall system energy is about the same. Therefore, T_1 and T_2 can be ruled out as the lone or dominant polytypes, though a superposition of the two of these (minidomains) or the addition of these with other polytpes could explain the lack of X/Y anisotropy of the CB minima.

Next, we consider more subtle but still clear effects in the data, especially the Rashba ‘minigaps’, wich are a deviation from the ‘classical’ type of Rashba splitting that is well-known for many materials. This Rashba minigap is most clear in the experimental panel c, with it being more filled in or fully absent for the other experimental cuts. To get a more quantitative calibration, a direct comparison is shown in Fig. 6, with the left panel showing the ARPES spectra and the right the DFT calculations. In Fig. 6a, it seems that the three polytypes T_1, T_2, and T_3 can provide satisfying agreements; however, it is clear in Fig. 6b that the T_3 polytype has to exist to match the experimental dispersions. Particularly, a direct comparison can be made between the band dispersions calculated in DFT and the experimental observation, even though there is some uncertainty due to the momentum broadening of the ARPES spectra. In Fig. 6d, the ARPES spectra show a minigap that seems to rule out a dominant T_1 structure.

On the other hand, in Fig. 6e, the ARPES somewhat resembles a Dirac cone, suggesting a crossing. However, the intensity near the crossing point is suppressed, indicating that a mini-gap is still present. The existence of the mini gap is better illustrated by the energy distribution curves (EDC) in Fig. 6c. Although the spectral intensity here shows a highly unconventional exponential energy dependence, there are clearly two broad peaks with a dip in between, corresponding to a minigap as predicted. The magnitude (around 0.015 eV) of the minigap can be estimated from the separation of the broad peaks (arrows), while the width of the peak introduces an uncertainty on the order of ±0.005 eV. While there are still considerable intensities inside the gap that might arise from strong impurity scattering, the magnitude of the gap is more consistent with the predictions of DFT on the T_2 and T_3 structures.

ARPES spectra along the Γ-Y cut, as shown in Fig. 4d and Fig. 6e, shows a suppression of spectral weight in the regime of the minigap, but there are also clearly states there as well. This would seem to favor a superposition of T_3 with any of T_0, T_1, T_2, all of which have the presence of "central states". The experimental momentum offsets (Marker II) are also tabulated in Table I, and are also most consistent wit the T_3 structure as the dominant polytype. To further investigate the possible mixing of different polytypes, in Fig. 7 we simulated the ARPES spectra from the DFT calculations with the Green's function, and introduced constant energy and momentum broadenings to mimic the quasiparticle scattering and instrumental resolution functions appropriate for our experimental setup. We have also incorporated an exponential energy dependence to the valence band intensities to approximately match the experimental observations. It can be seen that while T_3 simulation agrees best with experimental observation, a superposition of all three possibilities might match the data even better. However, it remains a challenge to fully account for all possible matrix element effects, which might have complex momentum and energy dependences.

As a summary, the data as a whole indicates that the T_3 structure contributes most significantly to the ARPES signal, with an additional T_1 and T_2 mixing as a secondary effect. This is in part a consequence of the geometric factor (our prediction that T_3 has double the occurrence possibility as T_1/T_2) as well as growth kinetics factors. A similar conclusion has been recently reached from the latest X-ray and neutron scattering results using very different but complementary metrics[28].

V. Discussion and Conclusion

Here we present a theory-guided approach to identify polytypes with subtle structural deviations (that are hard to identify with normal structural determination) via electronic markers, i.e., distinguishable

electronic properties because of the different structural or spin-orbit features, including especially crystal symmetries. The effect of the symmetry changing presented onto the electronic properties could be enhanced by other material-dependent factors. The most predominate marker in our work, the minigap in conduction and valence bands, is most strongly connected to the presence/breaking of non-symmorphic screw-axis symmetry at different wave vectors, with a smaller impact from SOC. This effect is analogous to the Peierls distortion, which drives a metallic system to be semiconducting by opening a gap because of the structural dimerization. Therefore, such an approach is not limited to the materials with large SOC, since the driving force of such marker is the change in structure and symmetry.

In conclusion, in this work we demonstrate the capability of ARPES to distinguish subtle electronic markers of different polytypes in the layered compound $LaOBiS_2$. We found that the ARPES spectra are mostly consistent with the system being largely the T_3 polytype, the knowledge of which might be crucial to our understanding of the novel properties in this system. While this work focused on a specific material, it demonstrated that different polytypes or a mixture of those can be generally identified by their relevant "electronic markers" with ARPES techniques. In the future, optical or transport experiments such as *interband* absorption and emission may also be utilized to observe or take advantage of such features, especially if the Fermi energy could be tuned to the middle of some of these Rashba minigaps.

Acknowledgements

This work was funded by NSF DMREF project DMR-1334170 to the University of Colorado and the University of Kentucky. We thank Feng Ye for help with some of the early structural characterizations of these materials. We thank Drs. S. K. Mo, Y. D. Chuang, J. D. Denlinger, N. C. Plumb and M. Shi for technical assistance on the ARPES measurements. The Advanced Light Source is supported by the Director, Office of Science, Office of Basic Energy Sciences, of the U.S. Department of Energy under Contract No. DE-AC02-05CH11231.

References:

1. Yeh, C.-Y.; Wei, S.-H.; Zunger, A. *Physical Review B* **1994,** 50, (4), 2715-2718.
2. Cheng, C.; Needs, R. J.; Heine, V. *Journal of Physics C: Solid State Physics* **1988,** 21, (6), 1049.
3. Yeh, C.-Y.; Lu, Z. W.; Froyen, S.; Zunger, A. *Physical Review B* **1992,** 46, (16), 10086-10097.
4. Patrick, L.; Hamilton, D. R.; Choyke, W. J. *Physical Review* **1966,** 143, (2), 526-536.

5. Nakamura, S. *Reviews of Modern Physics* **2015,** 87, (4), 1139-1151.
6. Geim, A. K.; Novoselov, K. S. *Nat Mater* **2007,** 6, (3), 183-191.
7. RadisavljevicB; RadenovicA; BrivioJ; GiacomettiV; KisA. *Nat Nano* **2011,** 6, (3), 147-150.
8. Hasan, M. Z.; Kane, C. L. *Reviews of Modern Physics* **2010,** 82, (4), 3045-3067.
9. Mizuguchi, Y.; Demura, S.; Deguchi, K.; Takano, Y.; Fujihisa, H.; Gotoh, Y.; Izawa, H.; Miura, O. *Journal of the Physical Society of Japan* **2012,** 81, (11).
10. Zhang, X.; Liu, Q.; Luo, J.-W.; Freeman, A. J.; Zunger, A. *Nat. Phys.* **2014,** 10, 387-393.
11. Liu, Q.; Zhang, X.; Jin, H.; Lam, K.; Im, J.; Freeman, A. J.; Zunger, A. *Physical Review B* **2015,** 91, (23), 235204.
12. Liu, Q.; Guo, Y.; Freeman, A. J. *Nano Letters* **2013,** 13, (11), 5264-5270.
13. Dong, X.-Y.; Wang, J.-F.; Zhang, R.-X.; Duan, W.-H.; Zhu, B.-F.; Sofo, J. O.; Liu, C.-X. *Nat Commun* **2015,** 6, 8517.
14. Tanryverdiev, V. S.; Aliev, O. M.; Aliev, I. I. *Inorganic Materials* **1995,** 31, 1497.
15. Lee, J.; Stone, M. B.; Huq, A.; Yildirim, T.; Ehlers, G.; Mizuguchi, Y.; Miura, O.; Takano, Y.; Deguchi, K.; Demura, S.; Lee, S. H. *Physical Review B* **2013,** 87, (20), 205134.
16. Zeng, L. K.; Wang, X. B.; Ma, J.; Richard, P.; Nie, S. M.; Weng, H. M.; Wang, N. L.; Wang, Z.; Qian, T.; Ding, H. *Physical Review B* **2014,** 90, (5), 054512.
17. Yildirim, T. *Physical Review B* **2013,** 87, (2), 020506.
18. Athauda, A.; Yang, J.; Lee, S.; Mizuguchi, Y.; Deguchi, K.; Takano, Y.; Miura, O.; Louca, D. *Physical Review B* **2015,** 91, (14), 144112.
19. Liu, Q.; Zhang, X.; Zunger, A. *Physical Review B* **2016,** 93, (17), 174119.
20. Kresse, G.; Joubert, D. *Phys. Rev. B* **1999,** 59, (3), 1758-1775.
21. Perdew, J. P.; Burke, K.; Ernzerhof, M. *Phys. Rev. Lett.* **1996,** 77, (18), 3865-3868.
22. A. Athauda, C. H., Y. Ren, S. Aswartham, J. Terzic, G. Cao, X. Zhu, D. Louca. *arXiv:1601.07517* **2016**.
23. Young, S. M.; Zaheer, S.; Teo, J. C. Y.; Kane, C. L.; Mele, E. J.; Rappe, A. M. *Physical Review Letters* **2012,** 108, (14), 140405.
24. Schoop, L. M.; Ali, M. N.; Straszer, C.; Topp, A.; Varykhalov, A.; Marchenko, D.; Duppel, V.; Parkin, S. S. P.; Lotsch, B. V.; Ast, C. R. *Nat Commun* **2016,** 7, 11696.
25. Ye, Z. R.; Yang, H. F.; Shen, D. W.; Jiang, J.; Niu, X. H.; Feng, D. L.; Du, Y. P.; Wan, X. G.; Liu, J. Z.; Zhu, X. Y.; Wen, H. H.; Jiang, M. H. *Physical Review B* **2014,** 90, (4), 045116.
26. Terashima, K.; Wakita, T.; Sunagawa, M.; Fujiwara, H.; Nagayama, T.; Ono, K.; Kumigashira, H.; Nagao, M.; Watauchi, S.; Tanaka, I.; Okazaki, H.; Takano, Y.; Mizuguchi, Y.; Usui, H.; Kuroki, K.; Muraoka, Y.; Yokoya, T. *Journal of Physics: Conference Series* **2016,** 683, (1), 012002.
27. Athauda, A.; Yang, J.; Li, B.; Mizuguchi, Y.; Lee, S.; Louca, D. *J Supercond Nov Magn* **2015,** 28, (4), 1255-1259.

Table I: Electronic markers of various polytypes T_0-T_3 and present experimental samples of $LaOBiS_2$. For the Rashba momentum offset, the two numbers indicate k_R along Γ-X(Y) and X(Y)-M. Subscript "e" and "h" stand for "electron" and "hole" respectively. Experimental values are estimated from peaks in energy distribution curves (EDC) and momentum distribution curves (MDC).

		T_0	T_1	T_2	T_3	Exptl.
Stacking form		---	(x, x)	(x, -x)	(x, y)	Unknown
Space group		P4/nmm	P21mn	P21/m	C2	Unknown
Inversion symmetry		Yes	No	Yes	No	No
Marker (i) (minigap energies)	Δ_{VB}(X) (eV)	0	0	0.16	0.11	0.15±0.05
	Δ_{VB}(Y) (eV)	0	0.03	0	0.11	0.15±0.05
	Δ_{CB}(X) (eV)	0	0	0.03	0.17	--
	Δ_{CB}(Y) (eV)	0	0.13	0	0.17	--
Marker (ii) Rashba momentum offsets)	$k_{R\text{-}e}$(X) (A^{-1})	0.047/0.017	0.034/0.039	0.005/0	0.041/0.039	0.045±0.08 /0.045±0.08
	$k_{R\text{-}h}$(X) (A^{-1})	0.047/0.036	0.043/0.029	0.010/0.010	0.056/0.028	0.06±0.01 /0.03±0.01
	$k_{R\text{-}e}$(Y) (A^{-1})	0.047/0.017	0.040/0.010	0.040/0.010	0.041/0.039	0.045±0.08 /0.045±0.08
	$k_{R\text{-}h}$(Y) (A^{-1})	0.047/0.036	0.068/0.038	0.059/0.040	0.056/0.028	0.09±0.03 /Unclear

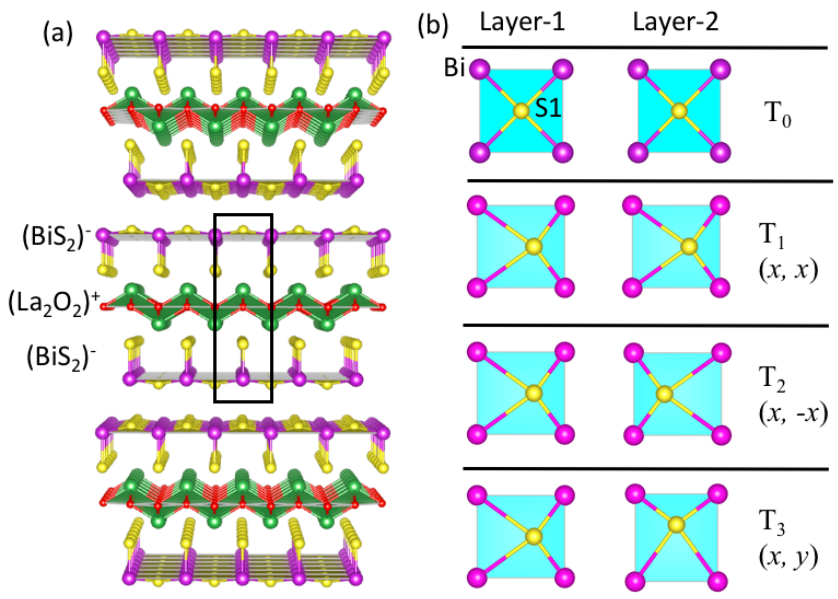

Fig: 1: (a) The layered structure of LaOBiS2 with the unit cell indicated by the black frame. The green, red, purple, and yellow balls represent La, O, Bi, and S atoms, respectively. Note that there are two BiS2 layers in each unit cell. (b) Different stacking configurations of two BiS2 layers for unstable structure T0 and its three stable polytypes T_1-T_3. Comparing with T0, the Bi-S1 2D networks of T_1-T_3 have an in-plane distortion showing the displacement of S1 atom along x or y direction, and thus two different Bi-S1 bond lengths.

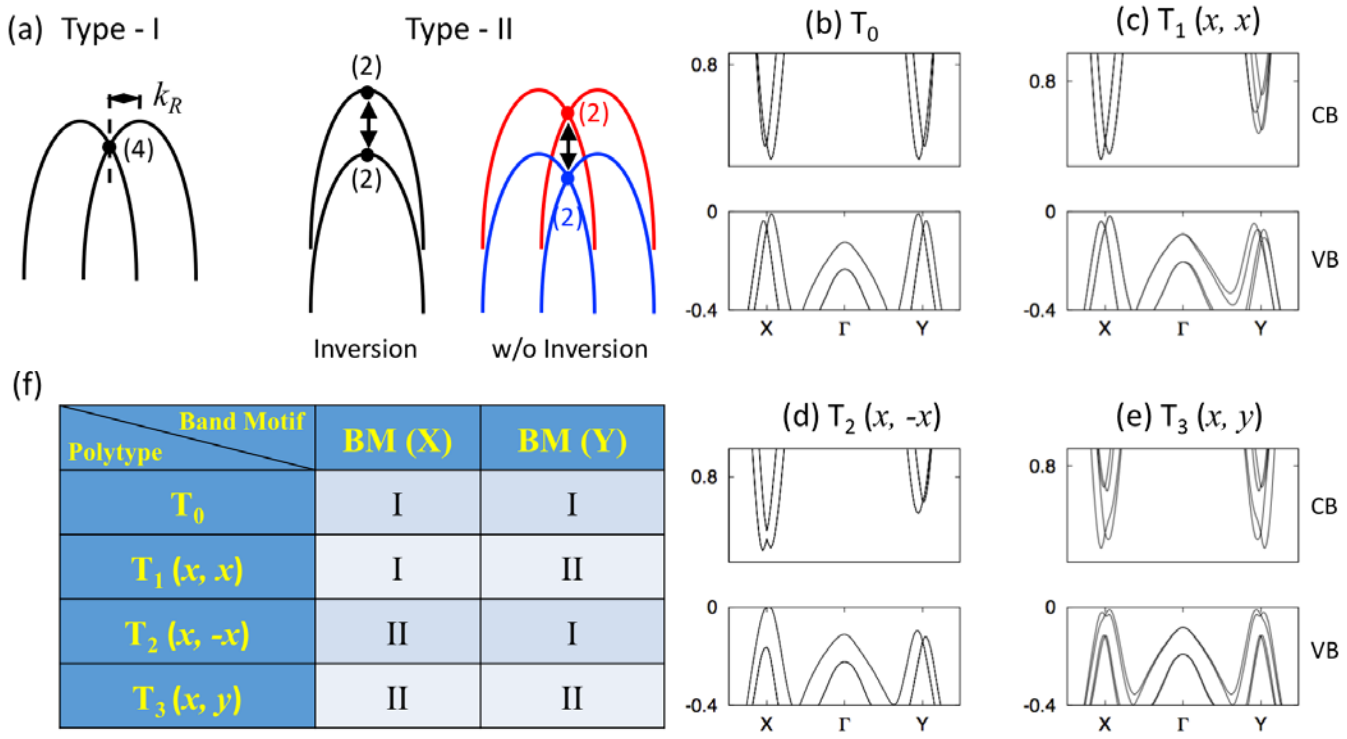

(f)

Band Motif / Polytype	BM (X)	BM (Y)
T_0	I	I
T_1 (x, x)	I	II
T_2 (x, -x)	II	I
T_3 (x, y)	II	II

Fig. 2: (a) Illustration of two types of band motifs (BM) classified by the degree of degeneracy (indicated by the number with parenthesis) at X (1/2, 0, 0) and Y (0, 1/2, 0) points. Type-I BM manifests the 4-fold degenerate Dirac point, which breaks into a pair of 2-fold degenerate points with a mini-gap Δ (horizontal arrows) as type-II BM. Off high-symmetry points X or Y type-II BM can have 2-fold degenerate bands (black) or single-degenerate bands (red and blue) according to the presence of inversion symmetry. (b-e) Band structures of T0-T3 polytypes show different BM types at X and Y point, which act as an electronic marker. Beyond the X or Y points in either direction of these plots is the M point. The BM types are summarized in (f).

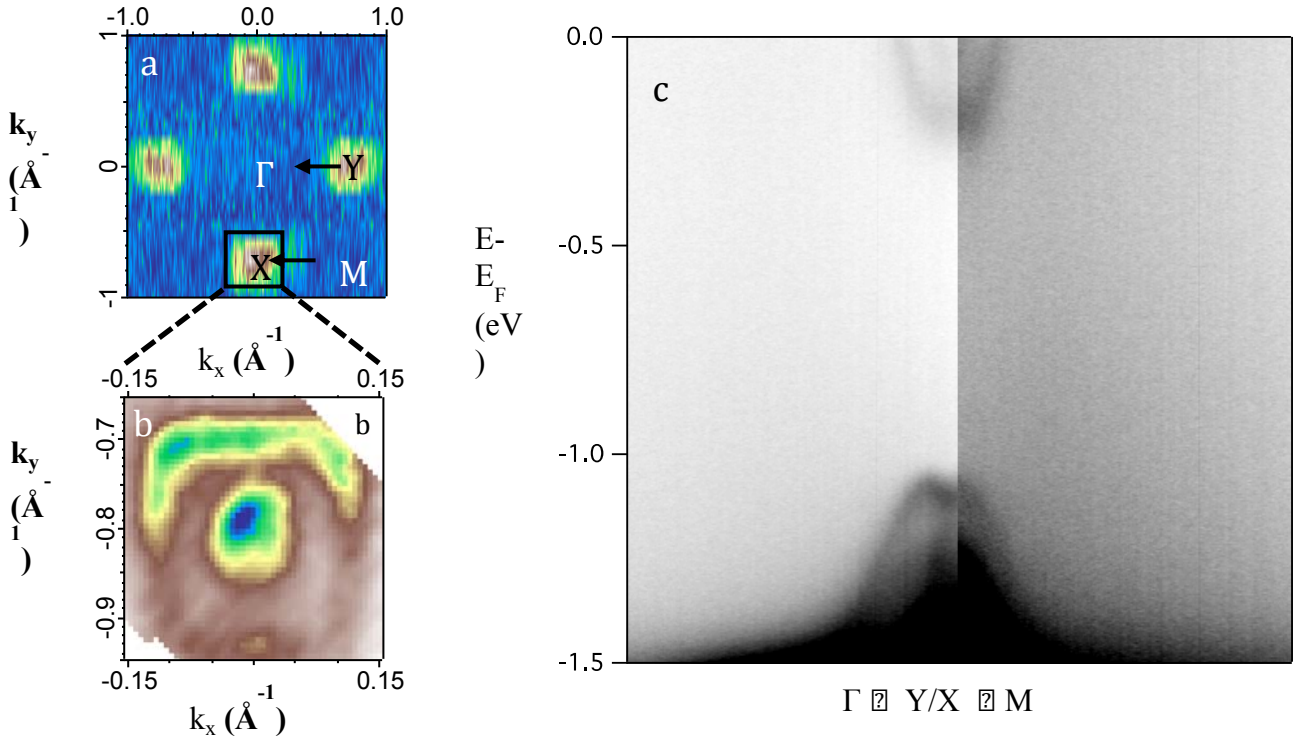

Fig. 3 a) Fermi map of lightly n-doped LaBiOS2 in the first Brillouin zone. Electron pockets are found near the X/Y points, the zoomed-in version of which is shown in b). ARPES spectra along high symmetry cut Γ-Y/X-M (black arrows) are shown in c) for conduction bands and valence band. The data is raw and unsymmetrized, taken under 60 eV, circular-left polarized light coming along Γ-Y with 45° incidence angle in Swisslight source beamline 9L. Similar data on 5 other samples were obtained at the Swiss Light Source beamline 9L as well as at the Advanced Light Source beamlines 4.0.3 and 10.0.1.

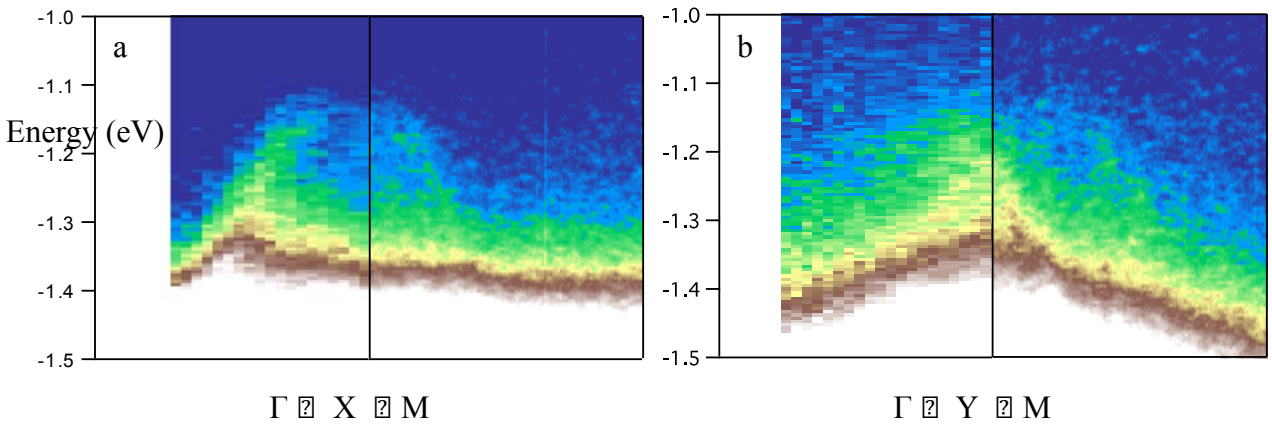

Fig. 4. ARPES spectra of the valence band near a) the “X” pocket and b) the “Y” pocket. Data were taken at ALS beam line 10.0.1 with 60 eV, linear horizontal polarized light coming in glancing angle along the Γ-X/ Γ-Y direction, with the sample’s azimuth angle rotated by 90° from a) to b).

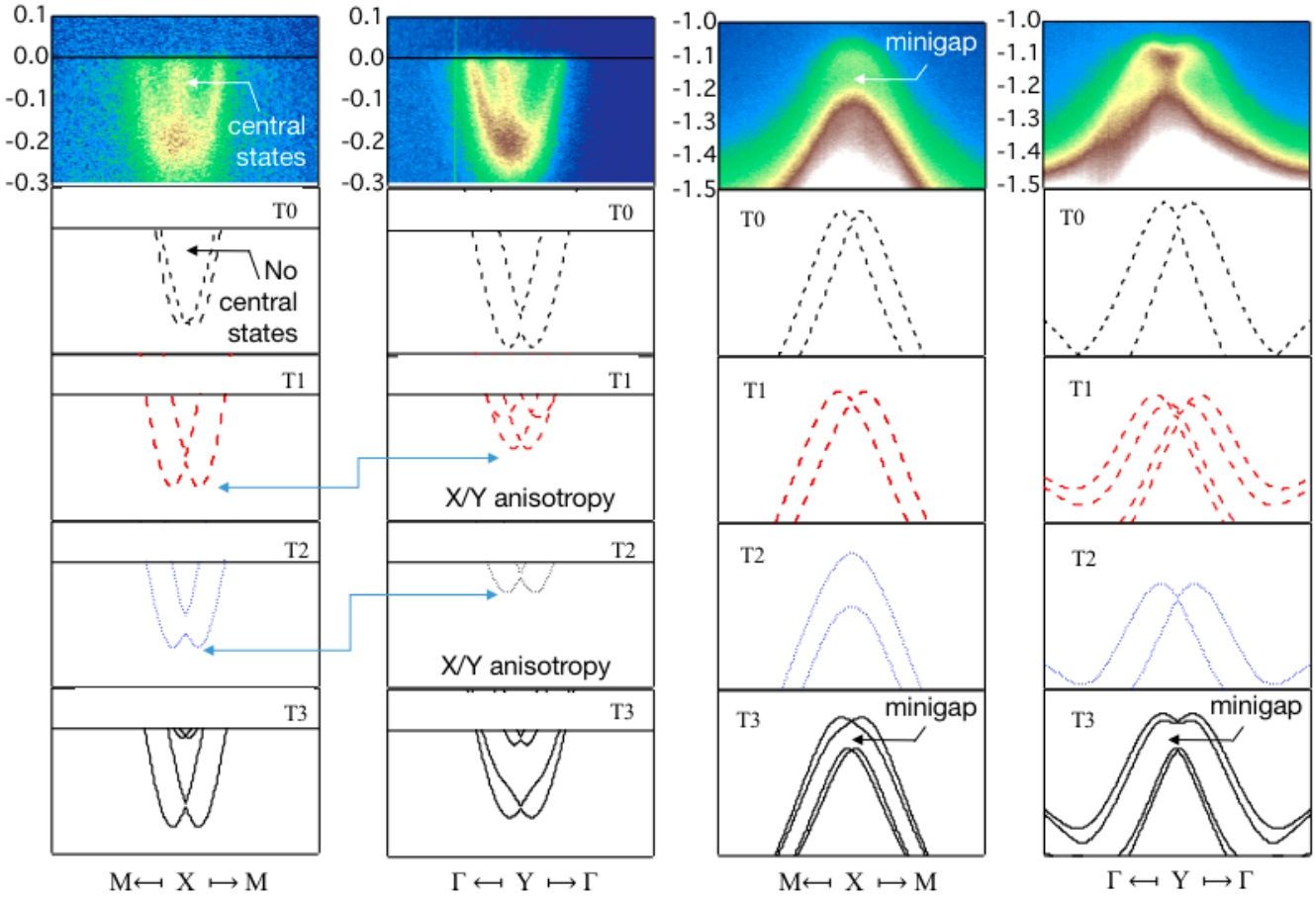

Fig. 5: Experimental spectra of a) conduction bands along M-X-M direction; b) conduction bands along Y-Γ-Y direction c) valence bands along M-X-M direction and d) valence bands along Y-Γ-Y direction, to be compared with DFT calculations of T0, T1, T2 and T3 respectively. ARPES spectra were taken under 60 eV, linear horizontal polarized light coming along Γ-Y direction with 45° incidence angle in Swiss Light Source beamline 9L. Similar data on 5 other samples were obtained at the Swiss Light Source beamline 9L as well as at the Advanced Light Source beamlines 4.0.3 and 10.0.1.

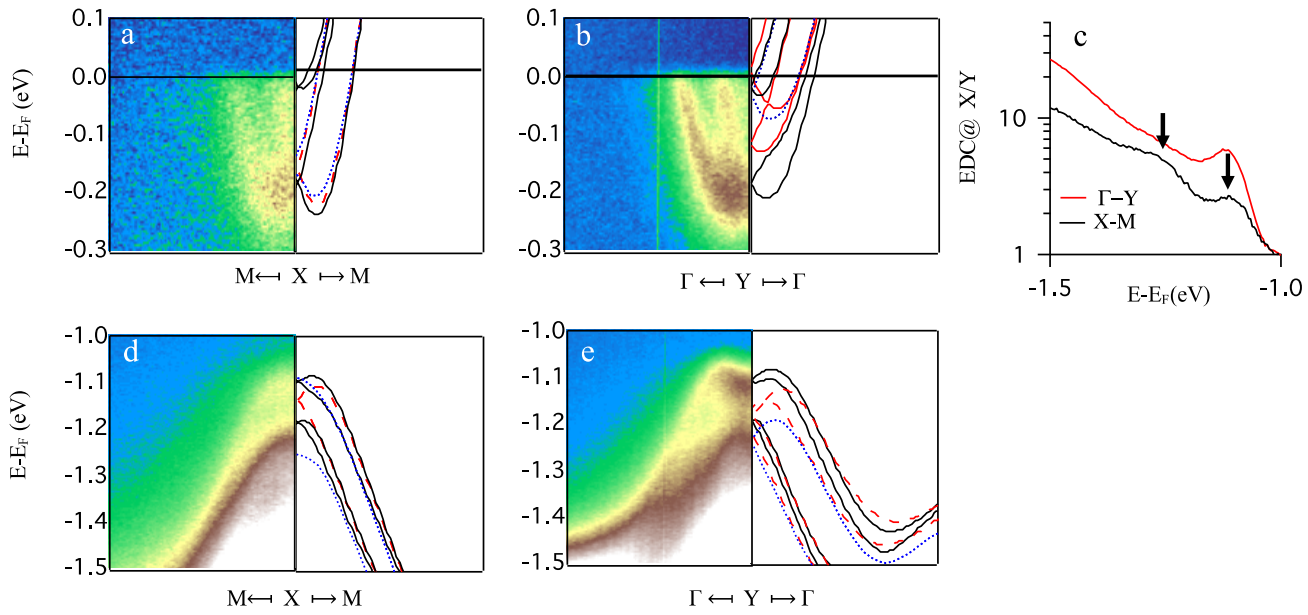

Fig. 6. ARPES spectra (left panel) of a) conduction bands along M-X-M cut; b) conduction bands along Γ-Y-Γ cut; d) valence bands along M-X-M cut and e) valencebands along Γ-Y-Γ cut, compared with DFT calculations (right panel) for T1 (red dash) and T2 (blue dot) and T3 (black solid) respectively. c) EDC at X/Y point, the local maxima of which should correspond to the dominant bands while the local minimum of which suggests the existence of gaping. The size of the minigap can be estimated from the distance between the two peaks.

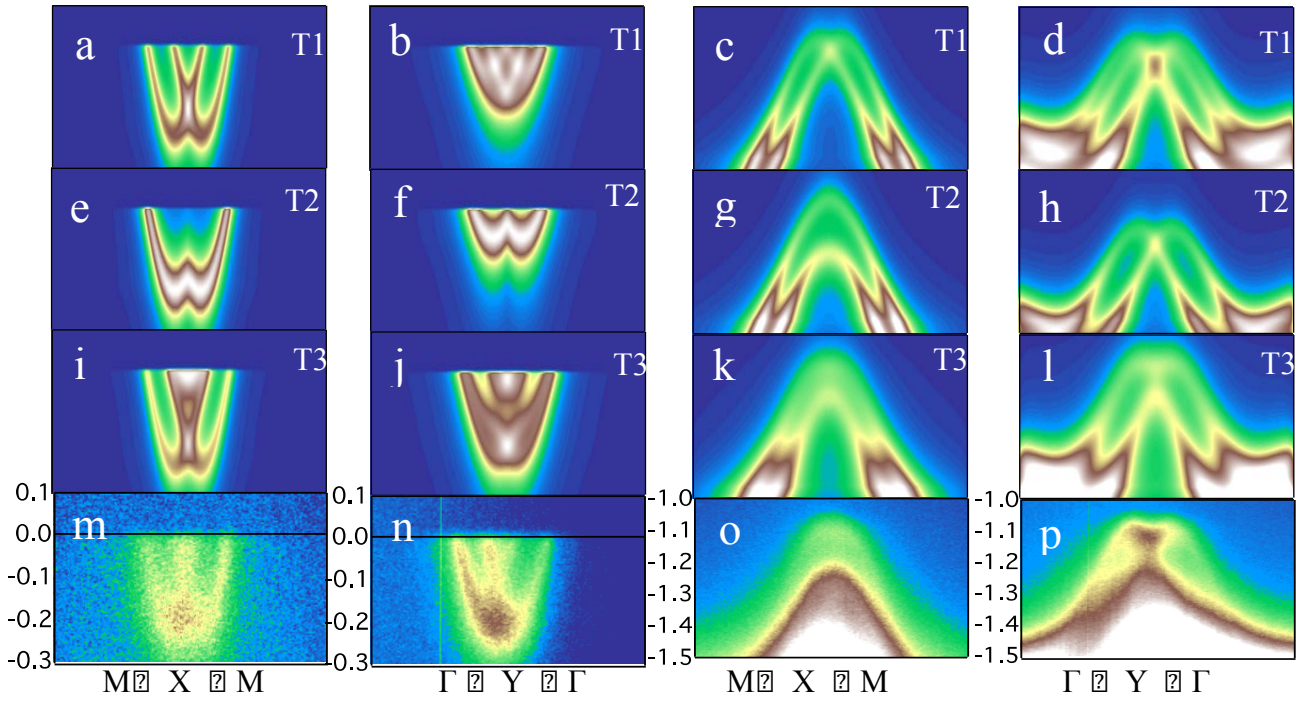

Fig. 7: Simulations of ARPES spectra for the T1, T2, and T3 polytypes (top three rows, respectively) compared to to ARPES data (bottom row). Left two columns – CB spectra along M-X-M and along Γ - Y- Γ. Right two columns: VB spectra along M-X-M and Γ-Y- Γ. All spectra in the bottom row were taken with 60 eV circular left polarized light coming along the Γ-Y direction at the Swiss Light Source beamline 9L.